TURBOLAB – TEST RIG DEMONSTRATOR FOR ELECTROMAGNETIC AND GEAR MESH DYNAMIC LOADS

Adrien PARPINEL, Vibratec, Ecully, France
Dr. Jessica NEUFOND, Vibratec, Ecully, France
Lionel DUVERMY, Vibratec, Ecully, France

Abstract

As part of the CORAC technological roadmap, the TURBOLAB project investigates design and modelling of hybrid turboprop systems. The integration of electric engine and gearbox on shaft line is not an easy task. Both are sources of dynamic loads, which must be fully apprehended to ensure shaft line integrity. As part of the development of numerical modelling methodology, a test rig is designed to replicate physical phenomena in a controlled environment. The shaft line 1st torsion mode is set at 42.5Hz. This demonstrator features a wide instrumentation to compose an experimental database of reference for next project tasks. Several test results are shared in this paper. Electric engine force harmonics are identified and quantified. The unbalanced magnetic pull is measured for several working points. The static and dynamic transmission errors from the gearbox are extracted and show how both gear mesh and electromagnetic torque ripple contribute to the transmission error.

1. INTRODUCTION

As part of the Civilian Aviation Research Council (CORAC) technological roadmap, the Research & Technology (R&T) TURBOLAB project contributes to the energy and competitiveness revolution.

Figure 1: CORAC and TURBOLAB logos

Preliminary to industrial applications, the project is related to other CORAC framework programs:

- Program DOPEE run by SAFRAN Aircraft Engines with technical aims to investigate electrical engine integration in turbofan architecture and build a demonstrator on a 1:1 scale.
- Hybrid turboprop program run by SAFRAN Helicopter Engines with aims to develop a new turboprop.

Aircraft and rotorcraft hybridization has regained interest as part of a global will to reduce greenhouse gas emissions. The automotive industry has already taken advantage of hybrid and fully electric propulsion systems. The aeronautic industry must face different technical challenges in order to safely use electric engines. The dynamic behavior of an electric engine is full of known phenomena. The electromagnetic dynamic pressures within the airgap can be estimated to predict the vibrations applied to the structure, as explained in Reference 1. Reference 2 discusses the changes in this dynamic excitation due to rotor eccentricities. Reference 3 proposes a test method on an automotive propulsion system, to measure the rotor eccentricity with optic sensors and correlate vibration levels with simulation results. While a weak coupling between electromagnetic and mechanical models serves the automotive sector's interests, the rotor dynamics at stake in aeronautics highlight concerns regarding possible strong coupling. Among these concerns, the unbalanced magnetic pull due to a dynamic eccentricity of the electric engine rotor needs to be correctly predicted for safety. Reference 4 presents research on strong coupling computation methods for electric engines in aeronautic ventilation systems. Few references report complete electromagnetic force test analyses in such industrial applications. Reference 5 presents one of the first measurement and correlation work on unbalanced magnetic pull due to a fractional slot to pole number ratio, on a standalone electric engine. Another example of a specific test rig for unbalanced magnetic pull due to rotor eccentricity can be found in Reference 6. However, it is not common to encounter publications of both force and vibration level measurements and correlation. The unbalanced magnetic pull effects on high-speed induction generator rotor dynamics are investigated in Reference 7 but mainly remain focused on vibration levels. Including an electric engine often requires a gearbox for engine vs shaft line speed adequacy. The trouble is that the gearbox itself is an additional source of complex dynamic excitations and an extra point of concern for shaft line torsional behavior, as developed in Reference 8.

The proposed paper advances the state of the art by sharing test results from R&T work conducted during the TURBOLAB project. The ultimate objective is to validate a simulation process that would make it possible to forecast dynamic risks to shaft line integrity, in the presence of an electric engine and a gearbox. For this purpose, a dynamic test rig, shown in Figure 2, was designed to replicate the dynamic effects at stake in a controlled environment, and to deliver a complete database essential for simulation process validation.

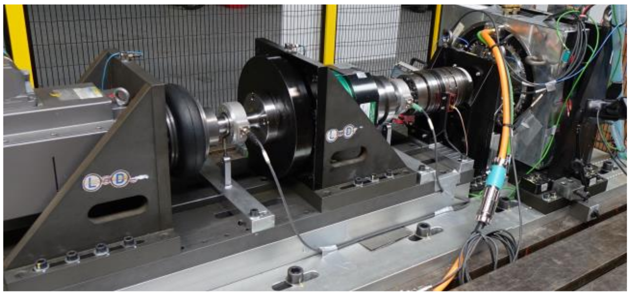

Figure 2: Picture of TURBOLAB test rig at Vibratec

The proposed paper briefly reports the test bench design work. A review of the instrumentation deployed on the test rig is proposed. Solutions for separate control of static and dynamic eccentricities are also presented. Main results from the conducted experimental plan are shared, featuring electromagnetic force harmonic measurements as well as the unbalanced magnetic pull. Gearbox transmission error is analyzed simultaneously. Rotor orbits are surveyed.

2. TEST RIG DEMONSTRATOR

2.1. Test rig design

The whole TURBOLAB test rig was designed with computed-aided design (CAD) and finite element model (FEM), as illustrated in Figure 3. The rig is built to test:

- Electric engine (MEL): synchronous permanent magnet motor 66 poles, 72 slots, 700N.m max torque, 600rpm max speed, 40kW max electrical power, 1.7mm airgap, 50mm length, 400mm outer diameter.
- Gearbox: epicyclic gear set, ratio 4, carrier with 3 planets, output torque 400N.m, 97% efficiency.

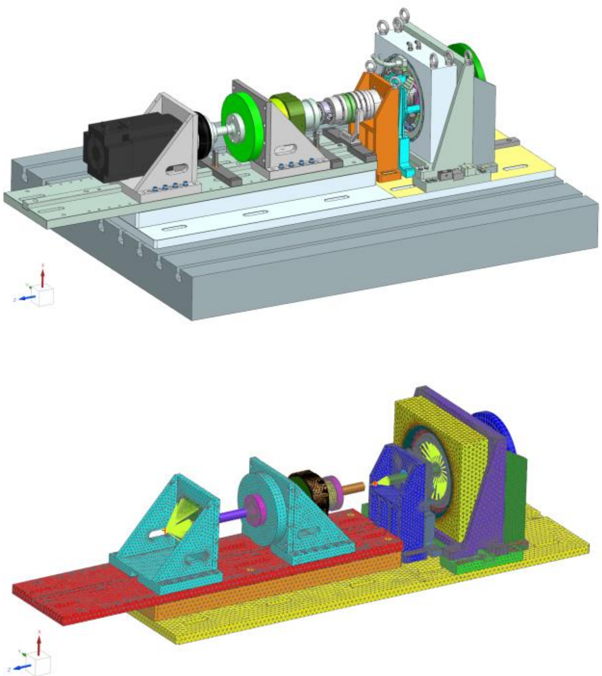

Figure 3: CAD (up) and FEM (down) models of the test bench

Test bench design must be addressed in order to correctly measure the dynamic effects. The test bench's eigenfrequencies limit the frequency range of measurements. Otherwise, the natural dynamics of the bench in operation might alter sensor signals. For example, the stator mounting was designed to allow measurement of electromagnetic forces up to 100Hz. The first bending mode of the stator mounting support, illustrated on Figure 4, was measured at around 155Hz.

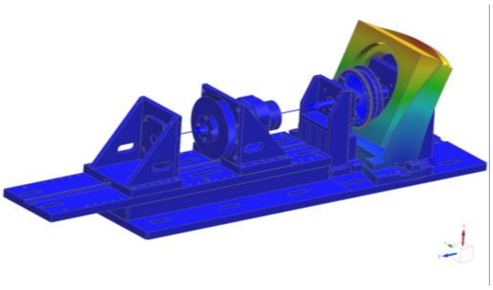

Figure 4: MEL stator mounting support bending mode, measured at around 155Hz

The FEM was used to validate the test bench design before manufacturing. Among the objectives of TURBOLAB projects, it was intended to work on a shaft line with its first torsion mode below 50Hz. The design of the test rig successfully sets this mode at 42.5Hz. First eigenfrequencies of shaft line modes, computed during design and measured on the test rig, are reported in Table *1*. Figure *5* to Figure *8* illustrate the corresponding modal deflection, computed with the FEM.

Table 1: Shaft line first modes

Shaft line mode	Model	Test rig	deviation
1st torsion	39.9Hz	42.5Hz	-6%
1st bending	112.0Hz	125.6Hz	-11%
2nd torsion	180.5Hz	184.5Hz	-2%
3rd torsion	385Hz	405Hz	-5%

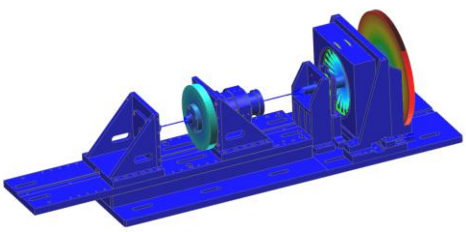

Figure 5: Illustration of 1st torsion mode measured at 42.5Hz

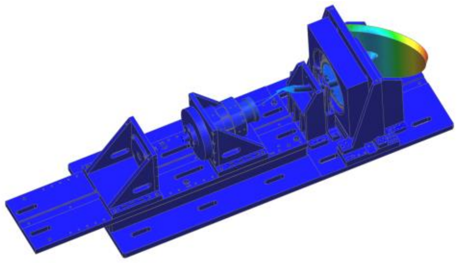

Figure 6: Illustration of 1st bending mode measured at 125.6Hz

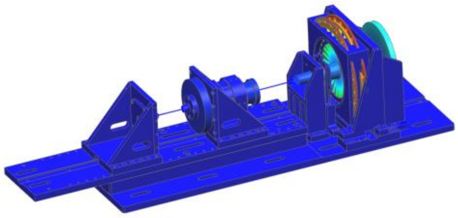

Figure 7: Illustration of 2nd torsion mode measured at 184.5Hz

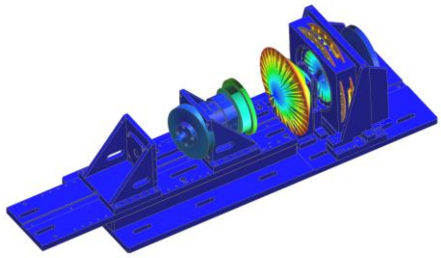

Figure 8: Illustration of 3rd torsion mode measured at 405Hz

The FEM used for design will also be used for TURBOLAB future work: dynamic response computation to electromagnetic and gearbox excitations.

2.2. Instrumentation overview

The instrumentation is rather diversified to allow a thorough analysis and return a complete test database:

- Torque evolution
- Forces applied to the MEL stator
- Gearbox transmission error
- Rotor radial and axial displacement
- MEL currents
- Accelerations at several locations

For this purpose, a torquemeter is installed on the shaft line, near the MEL. The forces applied to the stator are measured thanks to 4 piezoelectric force sensors, installed between the stator and its mounting support. The gearbox transmission error can be evaluated thanks to 2 incremental encoders placed upstream and downstream of the gearbox. The rotor axial and radial displacements are surveyed by a total of 6 laser displacement sensors. The MEL currents are measured with clamp ammeters. Accelerometers are placed along the structure to get vibration levels. The main instrumentation is shown on Figure *9*.

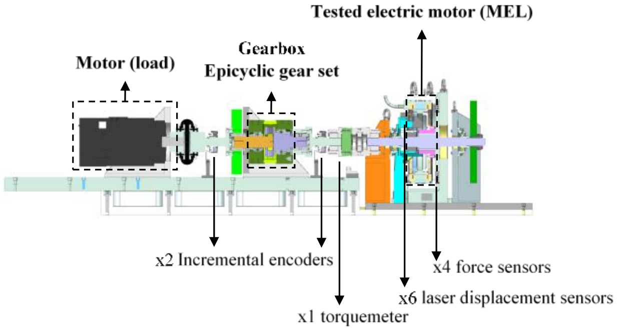

Figure 9: TURBOLAB test bench instrumentation overview

An experiment plan is defined and includes over 60 test configurations, combining several conditions:

- stationary or run-up MEL speed
- motor or generator mode of the MEL
- torque level
- eccentricity or not
- coincidences between harmonic excitation and particular structure frequencies
- etc.

The instrumentation set-up offers the possibility to measure different physics simultaneously. Once again, the first goal of this test rig is to return an experimental database of reference for numerical correlation and development of models.

2.3. Eccentricities control

It is important to highlight that the test bench is designed to include one system to control MEL static eccentricity and another system to control MEL dynamic eccentricity.

Eccentricities are illustrated on Figure *10*. In case of a static eccentricity, the rotor is not centered with the stator, but rotates around its own center. With a dynamic eccentricity, the rotor geometrical center is misaligned from stator, but the center of rotation remains on stator axis.

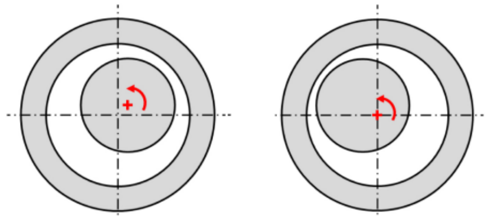
Figure 10: Illustration of static (left) and dynamic (right) eccentricities

The static eccentricity is controlled on the test rig by translation of the stator mounting support.

The dynamic eccentricity is controlled thanks a specific design of the MEL rotor mounting on the shaft line. The control system allows to change the MEL rotor geometrical axis, without changing the whole shaft line axis of rotation.

For both types of eccentricities, 3 levels are tested: 0.1, 0.2 and 0.3mm. These levels respectively represent around 5%, 11% and 17% of the MEL airgap length.

3. ELECTROMAGNETIC AND GEAR MESH LOADS

This chapter tends to give quick insight into dynamic loads studied with this test rig. On one hand, there is the electromagnetic load from the MEL, and on the other hand there is the gear mesh load.

3.1. Electromagnetic load

Within the electric engine, magnetic fields interaction is exploited to get torque. However, magnetic pressures apply to both rotor and stator interfaces in the airgap. These dynamic pressures are often decomposed into radial and tangential contributions. Both radial and tangential magnetic pressures are composed of several harmonic pressure waves. In other words, the electric engine not only produces torque, but also torque ripple and vibrations induced to the structure. The harmonic composition of these pressure waves is a direct consequence of the engine type, topology, winding scheme, and current harmonics.

A key element for anticipating this dynamic load is accessibility to electric engine data. This information is essential to build the electromagnetic model of the engine, as shown in Figure *11*.

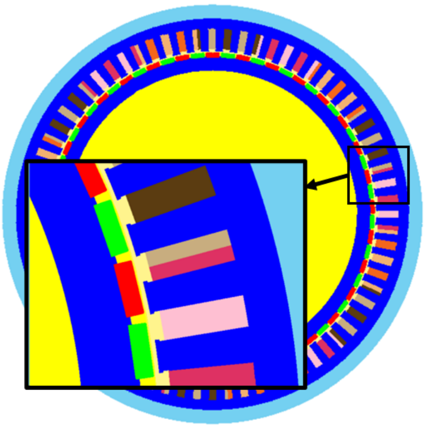

Figure 11: 2D electromagnetic model of the MEL

For the TURBOLAB project, the MEL installed on the test rig is an industrial purchase. Because all the necessary data for electromagnetic modelling was not available, a second engine was purchased for reverse engineering.

The electromagnetic model is handful to predict what is the electromagnetic excitation composed of. For example, the spatial and frequency composition of the tangential pressure waves of the MEL is shown in Figure *12*. For more details on this type of analysis, refer to Reference 1.

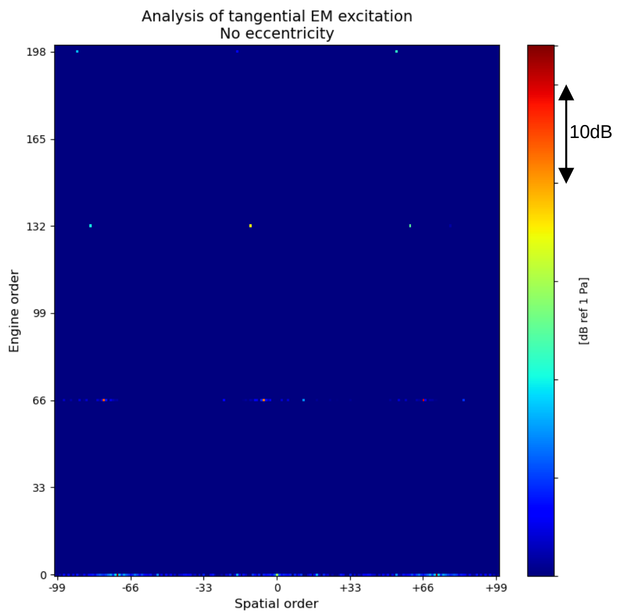

Figure 12: Example of spatial and frequency composition of electromagnetic excitation from MEL

Before running tests, the main frequencies of the dynamic load are known. For example, torque ripple from electromagnetic load is expected at engine orders 66, 132 and 198. The main harmonic of electromagnetic forces applied to the stator is engine order 66.

3.2. Gear mesh load

The integration of a gearbox on the shaft line must be addressed to anticipate several points. The gearbox itself is equivalent to an overall stiffness added on the shaft line. More importantly the gearbox is a source of dynamic excitations (see Reference 8), considering the transmission error and the variation of the mesh stiffness. Without mentioning nonlinear behaviors such as rattling or hammering noises, due to gear mesh contact loss, the whining noise is inherent to gearboxes. In most applications, the noise from the gearbox is the issue. In others, like TURBOLAB, the issue is the torsional source of excitation that the gearbox also represents. Furthermore, its interaction with the electric engine is verified.

As for electric engines, the dynamic load from the gearbox is linked to the topology of the system. It is important to insist that this topology relies on one hand on the macro geometry (modulus, number of teeth, etc.) and on the other hand on the micro geometry (teeth shape and corrections, static deflection, etc.).

Without macro geometry data, it is not possible to predict the dynamic load signature of the gearbox. Without the micro geometry data, the dynamic load cannot be quantified.

In TURBOLAB project, the gearbox design is fully known:

- Detailed CAD of the gearbox
- Macro geometry data
- Teeth micro geometry control report
- Experimental modal analysis of each component

The epicyclic gear set is illustrated on Figure *13*. The input shaft is connected to the sun, the output shaft is the carrier. There is no dephasing between planets meshes. The ring is fixed. The number of teeth is:

- $Z_s = 36$ (sun)
- $Z_p = 36$ (planet)
- $Z_r = 108$ (ring)

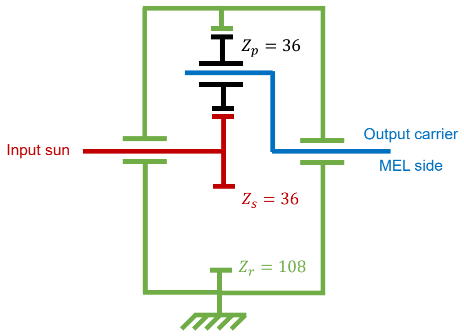

Figure 13: Illustration of the epicyclic gearbox installed on TURBOLAB test rig

The reduction ratio is 4. The meshing frequency f_{gear} is directly related to the carrier frequency rotation f_c by the number of ring teeth Z_r (Eq. 1).

$$f_{gear} = Z_r f_c \tag{1}$$

Hence, the main gear meshing frequencies expected with this gearbox are multiple of 108, relatively to carrier speed. Since the MEL is connected to the carrier side, it comes:

- Engine order 108: 1st meshing order
- Engine order 216: 2nd meshing order
- Engine order 324: 3rd meshing order

The preliminary knowledge of system characteristics is essential for test results analysis.

4. TORQUE AND TORSIONAL BEHAVIOR

The torque evolution is measured with the torquemeter. The experimental plan included several configurations of the test rig at stationary MEL speeds, as well as run-up sequences.

An example of torque analysis on a run-up sequence, is reported on Figure 14. The proposed figure includes:

- Torque time signal
- Spectrogram, with main engine orders written
- Engine order tracking along speeds
- Engine order tracking along frequencies
- Level tracking by frequency bands

During this sequence, the MEL works on motor mode at a constant 70N.m torque level, running up to 600rpm. The torque time signal is marked by a significant and constant torque ripple, besides clear amplifications.

To be noted, the high torque ripple levels are due to the proximity between the torquemeter location and a torsional vibration node. Even if the torquemeter

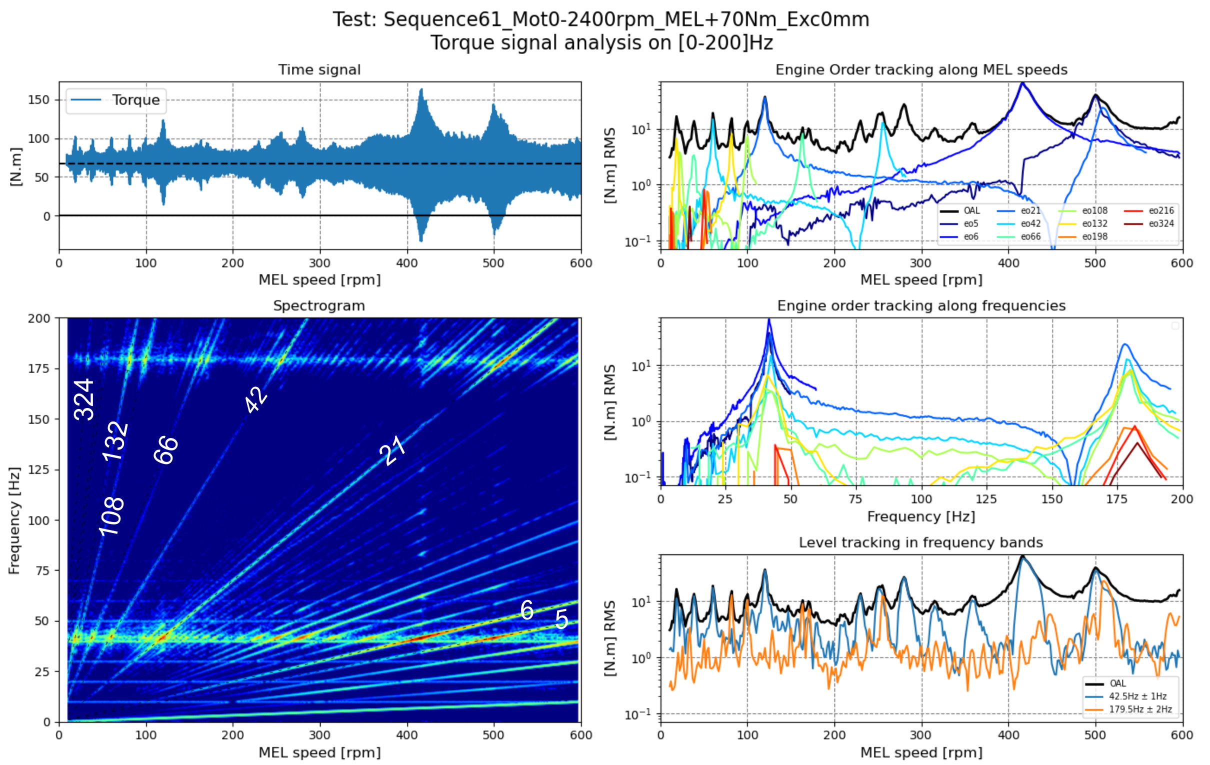

Figure 14: Torque analysis during MEL run-up to 600rpm, at 70N.m, on motor mode, without eccentricity

measures torque sign changes, that doesn't imply that the torque is varying as much in the gearbox. As a matter of fact, measurements with accelerometers confirm the continuity of teeth contact during tests.

The first two shaft line torsion modes can clearly be identified throughout the run-up on the spectrogram, around 42Hz and 180Hz. Any harmonic excitation, from MEL electromagnetics or gear mesh process, crossing these torsion frequencies amplifies the overall torque ripple.

The expected harmonics from MEL (engine orders 66, 132, 198) and from the gearbox (engine orders 108, 216, 324) cross the torsion modes at the beginning of the run-up, below 200rpm.

Other harmonics distinctly mark the torque signature and even lead to the highest levels of torque ripple: engine orders 5, 6, 21 and 42. The current work of TURBOLAB project does not explain yet the origin of these harmonic excitations. The excitation from the bearings is a direction for further investigations with numerical modelling.

5. FORCE MEASUREMENTS

5.1. Identification of force harmonics

For all tested configurations of the experiment plan, the signals from the force sensors are combined to evaluate the components of the overall force applied to the MEL stator. Focus is set on transverse components F_y and F_z, as radial forces are mainly applying.

For example, results for two test configurations are shared on Figure 15 (see next page), for a stationary MEL motor mode at 30rpm and 280N.m:

- Sequence #48: no eccentricity
- Sequence #54: 0.2mm dynamic eccentricity

Recomposed time signals of F_y and F_z are synchronized with MEL encoder, allowing to get evolution of force during one MEL rotor turn. Their mean synchronous value is evaluated and plotted in colors. The amplitude spectrum of signals are also plotted, revealing the harmonic content of these forces. This content is composed of electromagnetic harmonics.

In the case of sequence #48 without eccentricity, main MEL harmonics are found at engine orders 66, 132 and 198. Because of the diametrically asymmetrical winding of the MEL, there is also an unbalanced magnetic pull, even without rotor eccentricity. The level of unbalanced magnetic pull corresponds to the mean value of overall force F (Eq. 2), plotted in red on Figure 15. Here, the unbalanced magnetic pull is evaluated to 16.4N without eccentricity, and to 112.0N with 0.2mm eccentricity.

$$F = \sqrt{F_y^2 + F_z^2} \quad (2)$$

With dynamic eccentricity, the electromagnetic load is known to be affected (see Reference 2). Besides the unbalanced magnetic pull generated by this defect, extra harmonics are expected in the excitation, as modulations of initial electromagnetics pressure waves. For example, in this case, the dynamic eccentricity generates extra excitations at engine order 67. The main electromagnetic forces' harmonic values are tabulated in Table *2*.

Table 2: extract of MEL stator harmonic force amplitudes in [N] for test sequences #48 and #54.

[N]	Sequence #48 No eccentricity		Sequence #54 0.2mm dyn. ecc.	
	F_y	F_z	F_y	F_z
eo* 1	17,7	13,5	110,3	113,4
eo 65	0,2	0,2	0,2	0,3
eo 66	5,7	5,5	5,5	6,1
eo 67	0,9	0,9	5,1	4,7

*eo: engine order, relative to MEL speed

The force measurements for all tested configurations enhance the TURBOLAB experimental database with harmonic force values.

The absence of gear mesh process harmonics within the MEL stator forces comforts the idea that, on this test rig, the gearbox does not affect the electromagnetic forces.

As presented in the instrumentation of the test rig, several laser displacement sensors allow to measure the MEL rotor displacements. MEL rotor orbit is accessible for all tests. For sequences #48 and #54, the mean orbits are post-processed and reported on Figure *16* (see next page). The test rig design shows a great control of eccentricity; when the test rig is set-up to a 0.2 dynamic eccentricity, the mean measured orbit radius is 0.21mm.

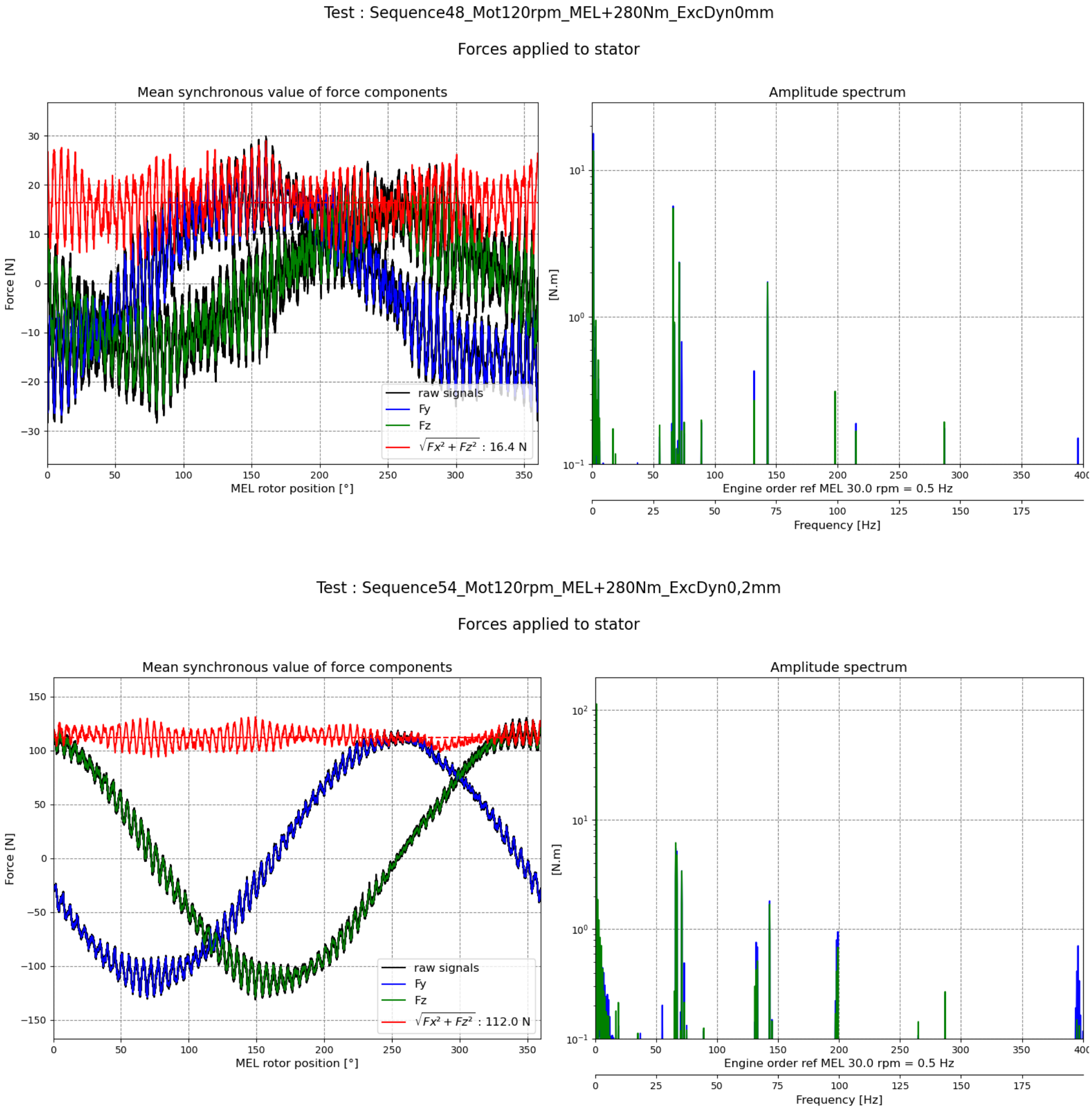

Figure 15 : MEL force measurements for 2 test configurations
Sequence #48 (up, no eccentricity) and Sequence #54 (down, 0.2mm dynamic eccentricity)

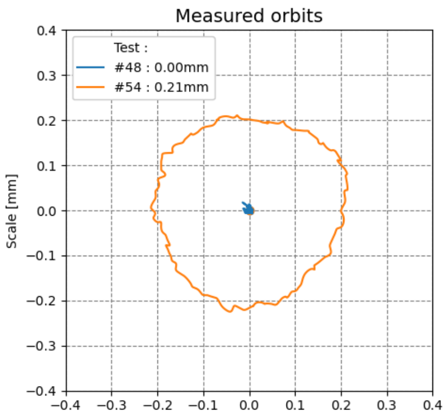

Figure 16: Mean measured MEL rotor orbits in [mm]
for test sequences #48 and #54

5.2. Unbalanced magnetic pull

Multiple test sequences for stationary engine speeds eventually made it possible to evaluate the unbalanced magnetic pull, from the tested MEL engine, for various levels of dynamic eccentricity on various working points. This is one of the main TURBOLAB project outputs, illustrated on Figure *17*. To be noted, the corresponding torque levels are not reported on Figure *17*, but vary from 10N.m to 280N.m. The x-axis with dynamic eccentricity level corresponds to the mean measured orbit radius of the MEL rotor.

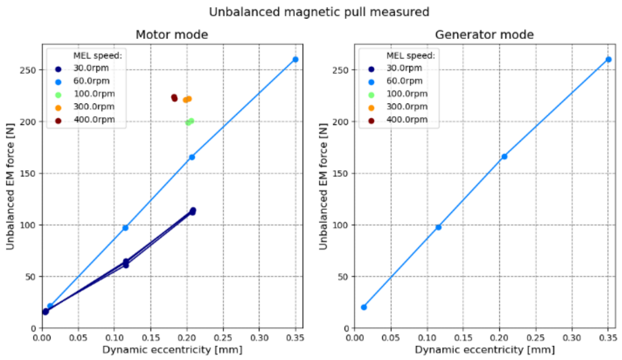

Figure 17: Unbalanced magnetic pull measured on TURBOLAB test rig

This important result, part of the TURBOLAB experimental database will serve as a reference for the numerical modelling developments. The prediction of unbalanced magnetic pull is essential in such applications where it can be more important than the mechanical unbalanced pull at low speeds. To give an idea, on TURBOLAB test rig, the dynamic eccentricity added leads to 15N at most, of mechanical unbalanced pull, whereas the magnetic pull goes over 250N.

6. TRANSMISSION ERROR MEASUREMENTS

6.1. Transmission error post-processing

The analysis of the transmission error from the gearbox returns information about the gear mesh load. For reminder, the transmission error is one of the internal sources of dynamic excitation from the gearbox. For such epicyclic gear set, only the overall transmission error can be accessed.

The transmission error is measured thanks to 2 incremental encoders placed upstream and downstream of the system, as shown on Figure *18*.

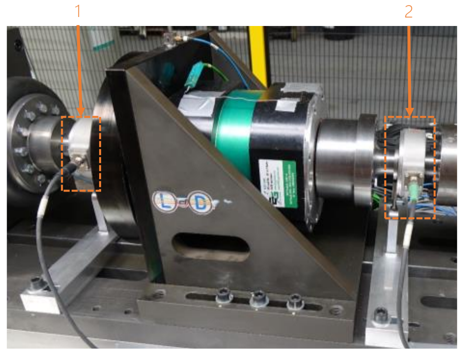

Figure 18: Incremental encoders around the gearbox

The encoders allow to measure the input and output angles of rotation. Figure *19* gives the example of encoders signals measured over time during a stationary engine speed test sequence. The number of fundamental periods evolution can be seen increasing, with ratio 4 between input and output. Each fundamental period here represents 48 turns of the sun. The acquisition duration is long enough to save several periods.

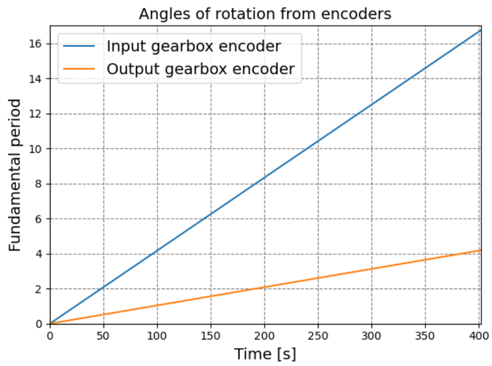

Figure 19: Example of angles measured from encoders

The transmission error simply results from the difference of encoders signals. The overall transmission error from angles on Figure *19* is reported on Figure *20*. The transmission error is plotted over a fundamental period. The duration of acquisition even allows to measure the mean synchronous value. The contributions of the encoders out-of-roundness can clearly be seen; 12 evolutions from output encoder and 48 evolutions from input encoder. The overall peak-to-peak (pk-pk) value is about 240µm, but not yet the value looked for since it includes encoders defects.

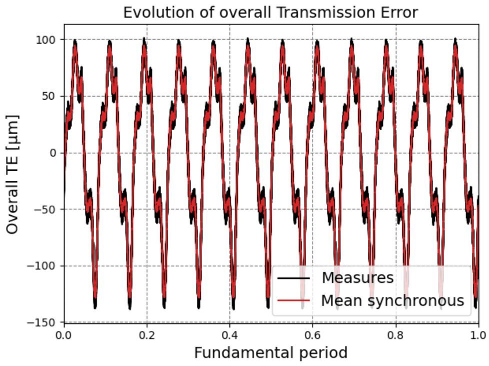

Figure 20: Example of overall raw transmission error

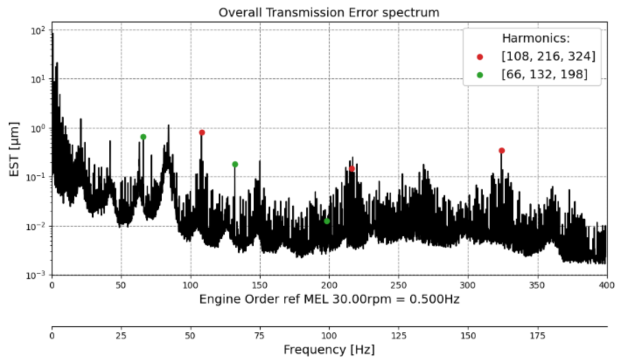

Figure 21: Example of amplitude spectrum of overall transmission error

To correctly analyze the transmission error, the amplitude spectrum should be computed. In this example, the spectrum is shown on Figure *21*. The frequency content becomes clearer. The encoders defects compose the low frequency content. The different harmonic contributions to the transmission error are identified at higher orders; gear mesh orders 108, 216 and 316 and MEL orders 66, 132 and 198. The spectrum also reveals the presence of the 1st torsion mode in the measured signals.

Based on this method, the transmission error can be analyzed by filtering the signal on specific harmonics.

6.2. STE measurement

The static transmission error (STE) is a source of excitation, characteristic of the gearbox. The STE corresponds to the transmission error of the gearbox, without any dynamic amplification. It is the physical quantity used to correlate and validate numerical models.

An example of STE analysis, from a stationary test sequence at 60rpm, is reported on Figure *21*. The torsion modes do not affect the amplitude of STE harmonics; STE can be evaluated from gear mesh harmonics only, or from MEL harmonics or from both.

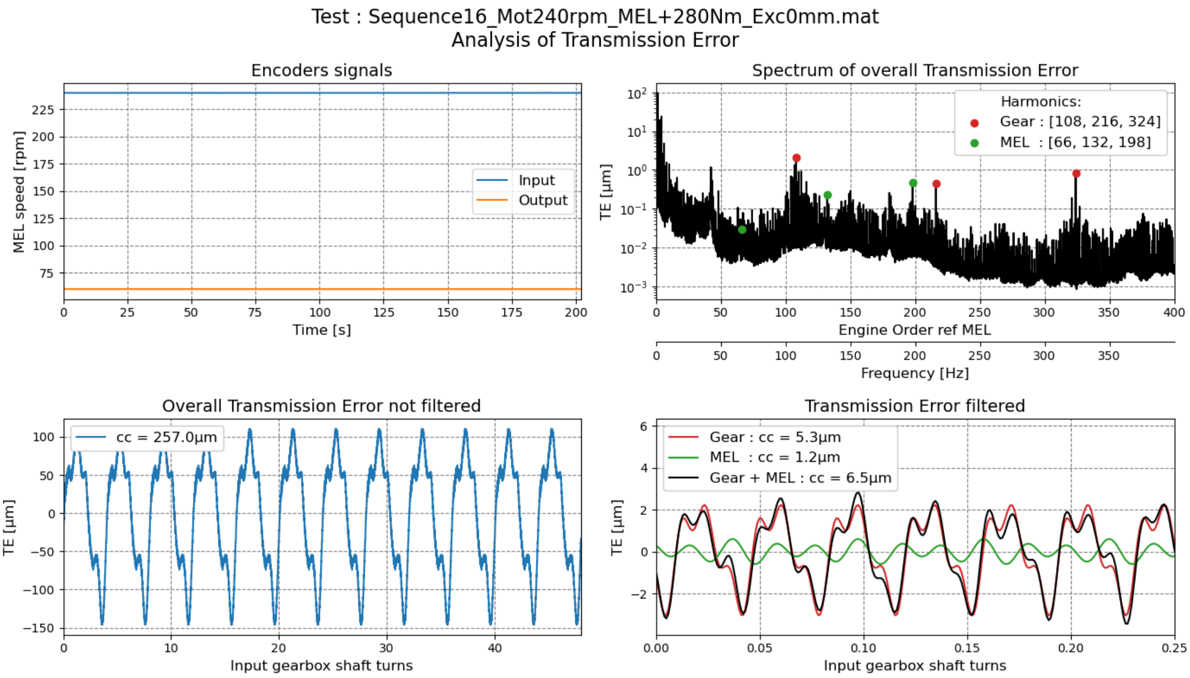

Figure 22: Example of STE measurement
Test sequence #16, MEL 60rpm, motor mode, 280N.m, no eccentricity

STE pk-pk value is eventually extracted from filtered signal.

For the record, a slow engine speed is not required to measure STE. Some tests were run at 7.5rpm during the experiment plan, but are not adequate since the 3rd meshing order (40.5Hz) is nearby the torsion mode (42.5Hz).

With several test sequences, STE values can be evaluated and saved in the database. For example, Figure *23* shares STE pk-pk levels measured for a stationary MEL speed of 60rpm, for several torque levels; negative torque means MEL generator mode, positive torque means MEL motor mode. From test results, it is noticed that here the STE pk-pk increases with torque. The increase is not the same whether the MEL is working as a generator or a motor. That shows how the load is not the same on the gearbox teeth depending on the working point. The gear contribution to STE is dominant compared to MEL harmonics.

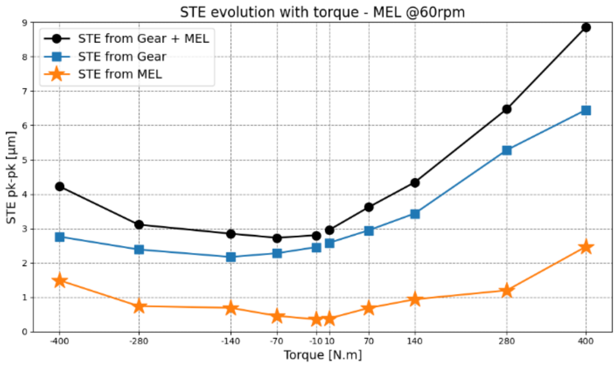

Figure 23: STE pk-pk measured for several MEL torque levels at 60rpm

The tracking of STE level can be completed with tracking of harmonic contributions. Figure *24* plots each contribution from MEL and gearbox, for the same working conditions as Figure *23*. The 1st meshing order (eo108) is the main contributor, followed by the 3rd meshing order (eo324). On this 60rpm working point, the engine order 198 from MEL becomes comparable to 3rd meshing order at 400N.m.

This data is valuable for correlation and validation of the numerical model deployed to replicate gearbox dynamic excitation on the shaft line.

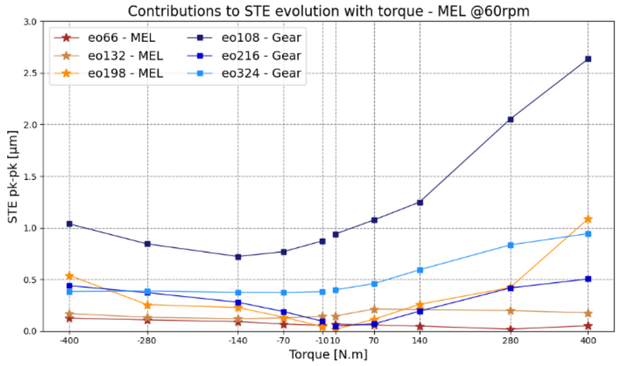

Figure 24: Evolution of harmonic contributions to STE pk-pk measured at 60rpm

6.3. DTE measurement

The transmission error can be tracked along run-up sequence. The approach used for stationary test sequences is adapted to run-up test sequences. Because the transmission error is affected by dynamic amplification, it is more convenient to talk about dynamic transmission error (DTE). The STE is the source of excitation, the DTE results from the system dynamic response.

For example, Figure 25 reports tracking of transmission error on test sequence #44. The MEL speed is swept from 0 to 600rpm, at a constant torque of 70N.m on motor mode, without any eccentricity.

The evolution of the transmission error pk-pk value along speeds is shown, considering MEL (eo66, eo132, eo198) and/or gearbox (eo108, eo216, eo324) harmonics. This distinction allows to identify whether the DTE is amplified by MEL or gearbox load. The amplifications correspond to coincidences with test rig eigenfrequencies. The synchronized plot of torque highlights that the peaks of torque ripple are not necessarily correlated to DTE peaks. The dynamic responses involved are different. DTE is amplified by several test rig structural modes, implicating the gearbox, whereas the torque ripple is amplified by torsion modes only. Interest for TURBOLAB work is focused on torsion modes rather than test rig structural modes.

Figure 25 also shares spectrogram of DTE. Added lines locate frequencies of the torsion modes. The order tracking completes the figure to identify, from gearbox and MEL harmonics, the main contributors to DTE pk-pk values. It should be remarked that the speed of the run-up limits the resolution of the analysis at low speeds. The faster the run-up, the less precise this type of post-processing is.

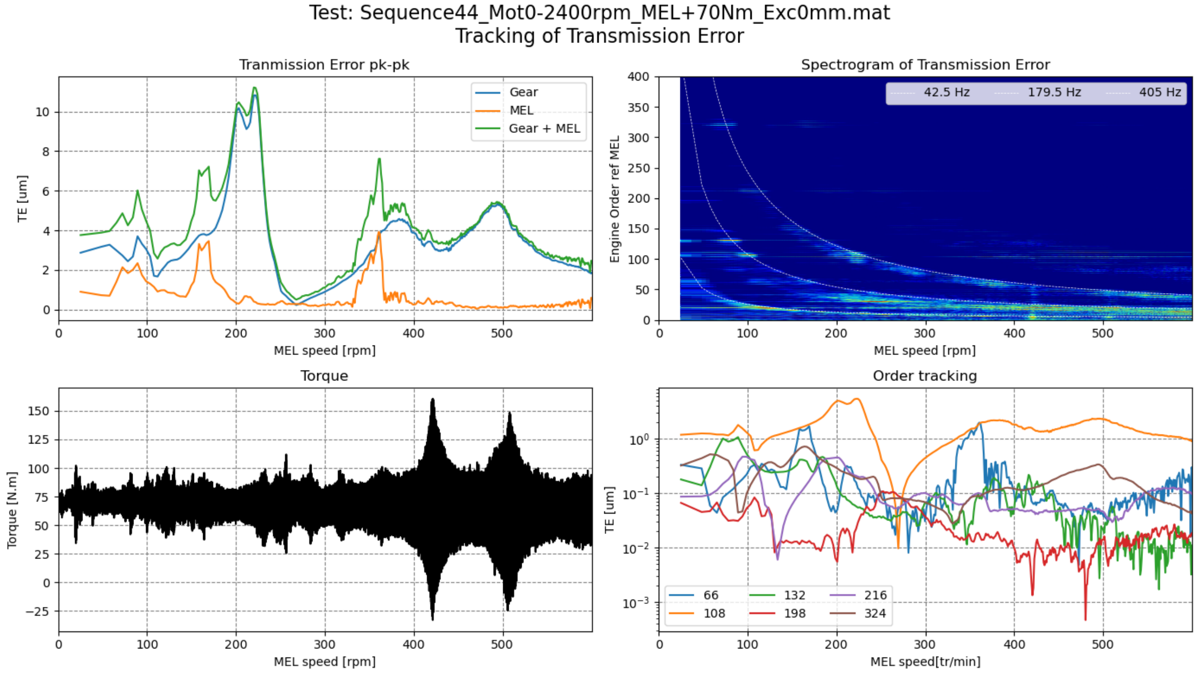

Figure 25: Example of Transmission Error tracking
Sequence #44, MEL run-up to 600rpm, 70N.m, motor mode, no eccentricity

The DTE analysis is repeated for several run-up test sequences from the experiment plan. Without detailing the specifications of test sequences, Figure *26* shows evolutions of DTE pk-pk level, from gearbox and MEL harmonics, along speeds. The working point of the MEL affects the gear mesh load and changes the DTE.

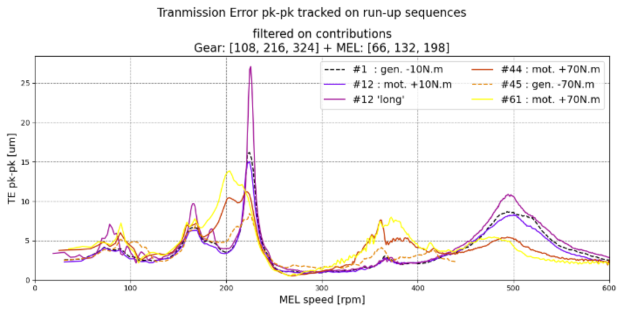

Figure 26: Evolution of DTE pk-pk for different run-up test sequences

Besides affecting the gear mesh load, it is interesting to witness how the MEL contribution to transmission error changes with working point. The relative contribution to transmission error is calculated from harmonics amplitude. For most test sequences from the experiment plan, the mesh process is the main contributor. However, some tested configurations see the MEL harmonics become the main contributors to the transmission error. Figure *27* compares the relative contribution to transmission error from gearbox harmonics (eo108, eo216, eo324) and MEL harmonics (eo66, eo132, eo198), for all stationary speed test sequences. In some cases, the MEL becomes the main contributor (60% to 70%) to the transmission error. For some cases, the MEL harmonics are amplified by test rig dynamics, in other cases, the electromagnetic working state of the MEL simply leads to high levels of torque ripple harmonics. This observation encourages to not only focus on mesh orders contributions to transmission error when designing the shaft line.

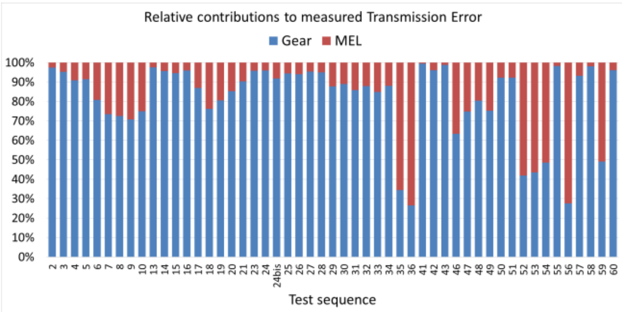

Figure 27: Comparison of gearbox and MEL relative contribution to pk-pk transmission error

7. CONCLUDING REMARKS

To conclude, this paper shares test results from TURBOLAB R&T project. The goal is to validate a numerical approach for hybrid shaft line modelling, in order to correctly predict loads from gear mesh process as well as from electromagnetics. As exposed in this paper:

1. A test rig demonstrator is designed to include an epicyclic gearbox and an electric engine, with control of eccentricities. The 1st torsion mode is below 50Hz.
2. A diverse instrumentation (torque, forces, incremental encoders, rotor displacements, currents, accelerations) is combined with an experiment plan to compose a database of reference.
3. The force measurements allow to identify and quantify electromagnetic harmonics from the electric engine.
4. The unbalanced magnetic pull is measured for several working points.
5. The transmission error from the gearbox, which is a characteristic of the gear mesh load, is tracked with encoders. Static transmission error and dynamic transmission error are studied separately.
6. The analysis of the actual transmission error on the test rig shows how the gear mesh is not always the main contributor and how the electric engine harmonics can become predominant in this source of excitation.
7. Next tasks of TURBOLAB project include correlation and validation of numerical models (gearbox, electric engine, full model of the test rig), based on the built database to develop modelling of such systems.

Authors contact:

Adrien PARPINEL, adrien.parpinel@vibratec.fr

Dr. Jessica NEUFOND, jessica.neufond@vibratec.fr

Lionel DUVERMY, lionel.duvermy@vibratec.fr

8. ACKNOWLEDGMENTS

The authors thank all the participants of the TURBOLAB project, as well as its contributors, DGAC via FRANCE 2030 investment plan organization, the European Union and SAFRAN Group. The authors also thank AKIRA Technologies Corporation for their implication and partnership in this project.

9. REFERENCES

1. Dupont, J., Bouvet, P., Wojtowicki, J., “Simulation of the Airborne and Structure-Borne Noise of Electric Powertrain: Validation of the Simulation Methodology”, SAE Technical Paper 2013-01-2005, 2013, doi:10.4271/2013-01-2005

2. Dupont, J., Aydoun, R., Bouvet, P., “Simulation of the Noise radiated by an Automotive Electric Motor: Influence of the Motor Defects”, *SAE Int. J. Alt. Power.* 3(2):310-320, 2014, doi:10.4271/2014-01-2070

3. Lecuru, S., Bouvet, P., Jouvray, J., and Wang, S., "Vibration Diagnosis on an Electric Motor: Use of Fiber Optic Sensors to Detect Rotor Eccentricity", SAE Technical Paper 2016-01-1836, 2016, doi:10.4271/2016-01-1836

4. Abdelnour, N., Caule, P., Lanfranchi, V., Chazot, J., "Contribution to the study of the electro-magneto-mechanic strong couplings for the acoustic and vibration of eletric motors of aeronautic ventilation systems", Forum Acusticum, 2020, Lyon, France, pp.1097-1098, ff10.48465/fa.2020.0504ff. ffhal-03235450

5. Z. Q. Zhu, D. Ishak, D. Howe and J. Chen, "Unbalanced Magnetic Forces in Permanent-Magnet Brushless Machines With Diametrically Asymmetric Phase Windings," in *IEEE Transactions on Industry Applications*, vol. 43, no. 6, pp. 1544-1553, Nov.-dec. 2007, doi: 10.1109/TIA.2007.908158

6. M. Michon, R. C. Holehouse, K. Atallah and J. Wang, "Unbalanced magnetic pull in permanent magnet machines," *7th IET International Conference on Power Electronics, Machines and Drives (PEMD 2014)*, Manchester, UK, 2014, pp. 1-6, doi: 10.1049/cp.2014.0277

7. H. Kim, E. Sikanen, J. Nerg, T. Sillanpää and J. T. Sopanen, "Unbalanced Magnetic Pull Effects on Rotordynamics of a High-Speed Induction Generator Supported by Active Magnetic Bearings – Analysis and Experimental Verification," in *IEEE Access*, vol. 8, pp. 212361-212370, 2020, doi: 10.1109/ACCESS.2020.3039629

8. Neufond, J., “Comportement dynamique et vibroacoustique des trains planétaires”, PhD thesis report, Ecole Centrale de Lyon, 2020